Neurobiology of Disease 142 (2020) 104955

Contents lists available at ScienceDirect

Neurobiology of Disease

journal homepage: www.elsevier.com/locate/ynbdi

# Prion protein post-translational modifications modulate heparan sulfate binding and limit aggregate size in prion disease

Julia A. Callender[a], Alejandro M. Sevillano[a,1], Katrin Soldau[a], Timothy D. Kurt[a,2], Taylor Schumann[a], Donald P. Pizzo[a], Hermann Altmeppen[b], Markus Glatzel[b], Jeffrey D. Esko[c], Christina J. Sigurdson[d,e,*]

[a] Departments of Pathology, UC San Diego, La Jolla, CA 92093, USA
[b] Institute of Neuropathology, University Medical Center Hamburg-Eppendorf (UKE), Hamburg, 20251, Germany
[c] Department of Cellular and Molecular Medicine, UC San Diego, La Jolla, CA 92093, USA
[d] Department of Pathology, Microbiology, and Immunology, UC Davis, Davis, CA 95616, USA
[e] Departments of Medicine, UC San Diego, La Jolla, CA 92093, USA

ARTICLE INFO

*Keywords:*
Amyloid
Neurodegeneration
Glycosaminoglycans
ADAM10 cleavage
Glycans
Glycosylation
Protein misfolding
Prion strains

ABSTRACT

Many aggregation-prone proteins linked to neurodegenerative disease are post-translationally modified during their biogenesis. *In vivo* pathogenesis studies have suggested that the presence of post-translational modifications can shift the aggregate assembly pathway and profoundly alter the disease phenotype. In prion disease, the N-linked glycans and GPI-anchor on the prion protein (PrP) impair fibril assembly. However, the relevance of the two glycans to aggregate structure and disease progression remains unclear. Here we show that prion-infected knockin mice expressing an additional PrP glycan (tri-glycosylated PrP) develop new plaque-like deposits on neuronal cell membranes, along the subarachnoid space, and periventricularly, suggestive of high prion mobility and transit through the interstitial fluid. These plaque-like deposits were largely non-congophilic and composed of full length, uncleaved PrP, indicating retention of the glycophosphatidylinositol (GPI) anchor. Prion aggregates sedimented in low density fractions following ultracentrifugation, consistent with oligomers, and bound low levels of heparan sulfate (HS) similar to other predominantly GPI-anchored prions. Collectively, these results suggest that highly glycosylated PrP primarily converts as a GPI-anchored glycoform, with low involvement of HS co-factors, limiting PrP assembly mainly to oligomers. Since $PrP^{C}$ is highly glycosylated, these findings may explain the high frequency of diffuse, synaptic, and plaque-like deposits in the brain as well as the rapid conversion commonly observed in human and animal prion disease.

## 1. Introduction

Protein aggregation and neuronal loss are defining features of neurodegenerative disease (Jucker and Walker, 2018; Kovacs, 2019; Vaquer-Alicea and Diamond, 2019), including prion disease (Baiardi et al., 2019). In prion disease, the clinical progression is extraordinarily rapid, with a median survival of approximately six months for patients with sporadic Creutzfeldt-Jakob disease (sCJD) (Iwasaki et al., 2017; Zerr and Parchi, 2018; Zerr et al., 2000). A causal role for the aggregated prion protein, $PrP^{Sc}$, in disease development has been established (Prusiner, 1982; Prusiner et al., 1990), supported most recently by studies showing disease induction from recombinant PrP fibrils (Burke et al., 2019; Deleault et al., 2007; Wang et al., 2010).

Compared to amyloid-β fibrils that display limited structural polymorphs (Selkoe, 1991), prion aggregates are remarkably diverse, forming a wide range of polymorphs (Sim and Caughey, 2008) and appearing histologically as diffuse, punctate, plaque-like, or congophilic plaques that vary in their biochemical properties (Bruce, 1993; Peretz et al., 2001). Similar to other proteins that aggregate in neurodegenerative disorders, PrP is post-translationally modified (Baldwin et al., 1990; Endo et al., 1989; Rudd et al., 2001; Srivastava et al., 2017; Srivastava et al., 2018; Stahl et al., 1991), yet how these post-translational modifications contribute to the aggregate conformation, co-factor interactions, and disease progression is unclear.

* Corresponding author at: Department of Pathology, UC San Diego, 9500 Gilman Dr., La Jolla, CA 92093-0612, USA.
*E-mail address:* csigurdson@ucsd.edu (C.J. Sigurdson).
[1] Current address: MD Anderson Cancer Center. 6767 Bertner St., 77030, Houston, TX.
[2] Current address: Foundation for Food and Agriculture Research, 401 9th St NW, Ste. 630, Washington, DC 20001, USA.

https://doi.org/10.1016/j.nbd.2020.104955
Received 10 April 2020; Received in revised form 9 May 2020; Accepted 21 May 2020
Available online 24 May 2020

$PrP^C$ is a ubiquitously expressed monomeric protein composed of 208 amino acids (Chesebro et al., 1985; Oesch et al., 1985) maintained in the outer plasma membrane by a glycophosphatidylinositol (GPI)-anchor (Baldwin et al., 1990; Rudd et al., 2001). The N-terminus is largely unstructured, whereas the C-terminal globular domain is composed of three α-helices with up to two N-linked glycans and a single disulfide bond that enhances protein stability (Riek et al., 1996). During prion disease, $PrP^C$ undergoes a major structural transformation from largely α-helical to β-sheet (Baron et al., 2011; Caughey et al., 1991b) in a conversion process templated by $PrP^{Sc}$ (Sandberg et al., 2011; Stohr et al., 2008).

Prion diseases are considered amyloid disorders, yet amyloid plaques composed of ultrastructurally visible fibrils are uncommon in sporadic human and animal prion disease (Greenlee and Greenlee, 2015; Zerr and Parchi, 2018). Notably, the prion protein is an atypical amyloidogenic protein, as it is relatively large, highly structured, glycosylated, and GPI-anchored. GPI-anchorless PrP aggregates assemble as fibrils in humans and in experimental models (Chesebro et al., 2005; Ghetti et al., 2018; Kim et al., 2018), suggesting that the GPI-anchor hinders fibril formation.

N-linked glycans may also limit PrP fibril formation. Glycans stabilize proteins (Culyba et al., 2011; Feng et al., 2018; Price et al., 2011), facilitate proper folding in the endoplasmic reticulum (Varki, 2017; Weerapana and Imperiali, 2006), and may impair fibril formation by shielding and stabilizing intramolecular disulfide bonds, as shown for a human PrP glycopeptide (175–195) (Bosques and Imperiali, 2003). Glycans may also decrease PrP interactions with anionic co-factors and potential scaffolds for fibril formation, such as sulfated glycosaminoglycans (Sevillano et al., 2020). However, glycans have also been shown to facilitate oligomer formation, depending on the chemical composition and location of the sugar present (Mitra et al., 2006).

Thus on the one hand, glycans may stabilize the tertiary structure of $PrP^C$, raising the energy barrier for conversion and prolonging survival time. On the other hand, glycans may hinder fibril elongation, restricting prions to small oligomers that transit readily through the brain thereby accelerating disease progression. To better understand the impact of PrP glycans on prion disease, we previously inoculated $Prnp^{187N}$ knockin mice, expressing triglycosylated $PrP^C$, with a fibrillar, plaque-forming prion strain known as mCWD (Sigurdson et al., 2006). Interestingly, the neuropathological phenotype switched from plaques to fine, granular $PrP^{Sc}$ deposits, and the survival time dropped by 60% as compared to infected wild type (WT) mice (Sevillano et al., 2020). Conversely, mice expressing unglycosylated PrP ($Prnp^{180Q,196Q}$) inoculated with non-plaque-forming prion strains instead developed large plaques (approximately 100 μm). Taken together, these findings suggest that glycans inhibit fibril formation. To help resolve the question of how PrP glycans on the carboxy terminus impact prion disease, here we inoculated $Prnp^{187N}$ mice with four prion strains and determined survival times and prion distribution in the brain and spinal cord. We used an antibody targeting ADAM10-cleaved PrP (Linsenmeier et al., 2018) to measure the cleaved $PrP^{Sc}$ levels, and mass spectrometry to measure the level and composition of prion-bound heparan sulfate (HS), which binds to plaque-forming prions (McBride et al., 1998; Sevillano et al., 2020; Snow et al., 1989a; Snow et al., 1990). We found that all four prion strains were readily converted and $Prnp^{187N}$ mice showed a similar or slightly longer survival time than in WT mice, yet with less spongiform change in the brain. Additionally, $Prnp^{187N}$ mice infected with two of four strains developed large plaque-like aggregates, which retained the GPI-anchor, bound low levels of HS, and sedimented in low density iodixanol fractions after ultracentrifugation, suggestive of smaller or less compact multimers. Finally, we compare our results to highly glycosylated human and animal prions, and propose a model for how glycans may underlie the extraordinary diversity in aggregate morphology and survival time in prion disease.

## 2. Materials and methods

### 2.1. $PrP^C$ expression in uninfected wild-type and $Prnp^{187N}$ brain

To measure total $PrP^C$ levels in WT (C57BL/6) and $Prnp^{187N}$ brain samples, 40 μg of 10% brain homogenate from uninfected mice was lysed in 2% N-lauryl sarcosine. Samples were then incubated for 15 min at 37 °C shaking at 1000 rpm. NuPage loading dye (Invitrogen) was added and samples were heated at 95 °C for 6 min prior to electrophoresis and transfer to nitrocellulose. Membranes were incubated in either anti-PrP antibody POM1 (epitope in the globular domain, amino acids 121–231 of the mouse PrP) (Polymenidou et al., 2008), $sPrP^{G228}$ antibody against ADAM10-cleaved PrP (neo-epitope at residue Gly228 (Linsenmeier et al., 2018)), or anti β-tubulin as a loading control (Cell Signaling Technology) and developed using chemiluminescent substrate. The chemiluminescent signals were captured and quantified using the Fuji LAS 4000 imager and Multigauge V3.0 software.

### 2.2. Structure modeling

Images were created using PyMol version 2.3.3. PrP crystal structure was obtained from PDB ID code 1AG2. N-linked glycans were modeled using the Glycam Glycoprotein Builder (Group. W, 2020). Tetra-antennary, sialic acid-containing N-linked glycans were chosen for the purposes of modeling due to evidence that the pool of PrP N-linked glycans contain bi-, tri-, and tetra-antennary glycans that contain primarily 2,6-linked sialic acid (Katorcha and Baskakov, 2017; Rudd et al., 1999).

### 2.3. Prion transmission experiments in mice

Groups of 4–11 male and female $Prnp^{187N}$ and WT (C57BL/6) mice were anesthetized with ketamine and xylazine and inoculated into the left parietal cortex with 30 μl of 1% prion-infected brain homogenate prepared from terminally ill mice. The prion strains used for inoculation were mouse-adapted RML, 22L, ME7, and mNS. The RML, 22L, and ME7 are cloned prion strains that have been maintained in C57BL/6 mice (Dickinson, 1976; Bruce and Dickinson, 1979; Dickinson et al., 1986; Aguzzi and Lakkaraju, 2016), while mNS inoculum was derived from repeated passage of a single scrapie-infected sheep brain (Aguzzi and Lakkaraju, 2016; Sigurdson et al., 2006) propagated in *tg*a20 and WT (C57BL/6) mice. For the serial passages of prions in $Prnp^{187N}$ mice, homogenates from individual mouse brains were used. As negative controls, groups of age-matched WT (C57BL/6) and $Prnp^{187N}$ mice ($n$ = 4–5 mice/ group) were inoculated intracerebrally with mock brain homogenate from uninfected WT mice and housed under the same conditions as the prion-infected mice.

Mice were maintained under specific pathogen-free conditions on a 12:12 light/dark cycle, and monitored three times weekly for the development of prion disease, including weight loss, ataxia, kyphosis, stiff tail, hind leg clasp, and hind leg paresis. Mice were euthanized at the onset of terminal clinical signs, and the incubation period was calculated from the day of inoculation to the day of terminal clinical disease. During the necropsy, one hemispheres was formalin-fixed, then immersed in 96–98% formic acid for 1 h, washed in water, and post-fixed in formalin for 2–4 days. Hemi-brains were then cut into 2 mm transverse sections and paraffin-embedded for histological analysis. The remaining brain sections were frozen for biochemical analyses.

### 2.4. Histopathology and immunohistochemical stains

Four micron sections were cut onto positively charged sialinized glass slides and stained with hematoxylin and eosin (HE), or immunostained using antibodies for total PrP (SAF84)(Cayman Chemical), astrocytes (glial fibrillary acidic protein, GFAP)(DAKO), and heparan sulfate (10E4)(AMS Bioscience). PrP (SAF84; 1:400) and GFAP

immunolabelling (1:6000) was performed on an automated tissue immunostainer (Ventana Discovery Ultra, Ventana Medical Systems, Inc) with antigen retrieval performed by heating sections in a Tris-based EDTA buffer at 95 °C for 92 min or using a protease treatment (P2, Ventana) for 16 min, respectively. For HS immunolabelling, epitope retrieval was performed by placing sections in citrate buffer (pH 6), heating in a pressure cooker for 20 min, cooling for 5 min, and washing in distilled water. Sections were blocked and incubated with anti-heparan sulfate antibody for 45 min followed by anti-mouse biotin (Jackson Immunolabs; 1:250) for 30 min and then streptavidin-HRP (Jackson Immunoresearch) for 45 min. Slides were then incubated with DAB reagent (Thermo Scientific) for 15 min. Sections were counterstained with hematoxylin. Control slides for the HS stain were treated with heparin lyases I,II, III at 37 °C for 60 min prior to immunoIabelling. To quantify plaque size in ME7 and mNS-infected mice, brain sections containing plaques were imaged at high magnification (400×) and the diameter at the largest point of the plaque was measured using ImageJ software ($N \geq 35$ plaques or plaque-like deposits from three mice per group).

For the Congo red staining, slides were deparaffinized, fixed in 70% ethanol for 10 min, immersed in an alkaline solution and then stained with Congo red solution overnight.

For the CD9 and total PrP co-immunostain of brain sections, epitope retrieval was first performed by immersing the sections in 96% formic acid for 5 min, digesting sections with 5 μg/ml PK for 10 min, and then heating slides in citrate buffer within a pressure cooker for 20 min, washing slides between each step. CD9 and PrP were labelled using anti-CD9 and anti-PrP antibodies (CD9: Novus; PrP: SAF84 from Cayman Chemical), and then sequentially, anti-rabbit HRP followed by tyramide-Alexa488 followed by anti-mouse CY3, to label CD9 and PrP, respectively.

### 2.5. Lesion profile

Brain lesions from prion-infected WT (C57BL/6) and *Prnp*$^{187N}$ mice were scored for the level of spongiosis, gliosis, and PrP immunological reactivity on a scale of 0–3 (0 = not detectable, 1 = mild, 2 = moderate, 3 = severe) in 7 regions including grey and white matter: (1) dorsal medulla, (2) cerebellum, (3) hypothalamus, (4) medial thalamus, (5) hippocampus, (6) medial cerebral cortex dorsal to hippocampus, and (7) cerebral peduncle. A sum of the three scores resulted in the value obtained for the lesion profile for the individual animal and was depicted in the 'radar plots'. Two investigators blinded to animal identification performed the histological analyses. Groups of 4–6 mice were analyzed for each strain.

### 2.6. PK-resistant PrP$^{Sc}$ analyses

Brain homogenates were lysed in 2% N-lauryl sarcosine in PBS and incubated in PBS or digested with 50 μg/ml PK for 30 min at 37 °C prior to western blotting. Membranes were incubated with monoclonal antibody POM1, POM19 (epitope in the globular domain), POM2 (epitope: 57–64, 64–72, 72–80 and 80–88), or POM3 (epitope: 95–100) where indicated (Polymenidou et al., 2008).

For measuring shed PrP$^{Sc}$ by western blot, PrP$^{Sc}$ from ME7- and mNS-infected *Prnp*$^{187N}$ mice and mCWD-infected mice was concentrated from 10% brain homogenate by performing sodium phosphotungstic acid precipitation prior to western blotting (Wadsworth et al., 2001). In brief, 10% brain homogenate in an equal volume of 4% sarkosyl in PBS was digested with benzonase™ (Sigma) followed by treatment with 100 μg/ml PK at 37 °C for 30 min. After addition of 4% sodium phosphotungstic acid in 170 mM $MgCl_2$ and protease inhibitors (Complete™, Roche), extracts were incubated at 37 °C for 30 min and centrifuged at 18,000 *g* for 30 min at 25 °C. Pellets were resuspended in 2% N-lauryl sarcosine prior to electrophoresis and immunoblotting. Membranes were incubated with monoclonal antibody POM19 (Polymenidou et al., 2008) or polyclonal antibody sPrP$^{G228}$ (Linsenmeier et al., 2018) followed by incubation with an HRP-conjugated IgG secondary antibody. The blots were developed using a chemiluminescent substrate (Supersignal West Dura ECL, ThermoFisher Scientific) and visualized on a Fuji LAS 4000 imager. Quantification of PrP$^{Sc}$ glycoforms and total PrP$^{Sc}$ was performed using Multigauge V3 software (Fujifilm).

### 2.7. Velocity sedimentation

Brain homogenate [10% in PBS (*w/v*)] from WT (C57BL/6) or *Prnp*$^{187N}$ mice was lysed in velocity sedimentation lysis buffer (100 mM Tris-HCl pH 7.5, 150 mM NaCl, 1% N-lauryl sarcosine, final) for 30 min, carefully placed over a 4–24% step gradient (4%, 8%, 12%, 16%, 20%, and 24%), and centrifuged at 150,000 *g* for 1 h. Fourteen fractions were collected from each tube, with the final fraction including the resuspended pellet. Aliquots of each fraction were digested with 50 μg/ml of PK for 30 min at 37 °C prior to immunoblotting and probing with anti-PrP antibody, POM19 (Polymenidou et al., 2008).

### 2.8. Purification of PrP$^{Sc}$ for mass spectrometry studies

PrP$^{Sc}$ was purified from mouse brain following previously described procedures (Raymond and Chabry, 2004), with minor modifications. 10% brain homogenate was mixed with an equal volume of TEN(D) buffer [5% sarkosyl in 50 mM Tris-HCl, 5 mM EDTA, 665 mM NaCl, 0.2 mM dithiothreitol, pH 8.0), containing complete™ protease inhibitors (Roche)] and incubated on ice for 1 h prior to centrifugation at 18,000 *g* for 30 min at 4 °C. All but 100 μl of supernatant was removed, and the pellet was resuspended in 100 μl of residual supernatant and diluted to 1 ml with 10% sarkosyl TEN(D). Each supernatant and pellet was incubated for 30 min on ice and then centrifuged at 22,000 *g* for 30 min at 4 °C. Supernatants were recovered while pellets were held on ice. Supernatants were added to ultracentrifuge tubes with 10% N-lauryl sarcosine TEN(D) buffer containing protease inhibitors and centrifuged at 150,000 *g* for 2.5 h at 4 °C. Supernatants were discarded while pellets were rinsed with 100 μl of 10% NaCl in TEN(D) buffer with 1% sulfobetaine (SB3–14) and protease inhibitors and then combined with pellets and centrifuged at 225,000 *g* for 2 h at 20 °C. The supernatant was discarded and pellet was washed and then resuspended in ice cold TMS buffer containing protease inhibitors (10 mM Tris-HCl, 5 mM $MgCl_2$, 100 mM NaCl, pH 7.0). Samples were incubated on ice overnight at 4 °C. Samples were then incubated with 25 units/ml benzonase™ (Sigma-Aldrich) and 50 mM $MgCl_2$ for 30 min at 37 °C followed by a digestion with 10 μg/ml PK for 1 h at 37 °C. PK digestion was stopped by incubating samples with 2 mM PMSF on ice for 15 min. Samples were incubated with 20 mM EDTA for 15 min at 37 °C. An equal volume of 20% NaCl was added to all tubes followed by an equal volume of 2% SB3–14 buffer. For the sucrose gradient, a layer of 0.5 M sucrose in buffer [100 mM NaCl, 10 mM Tris, and 0.5% SB3–14 (pH 7.4)] was added to ultracentrifuge tubes. Samples were then carefully overlaid on a sucrose layer and the tubes topped with TMS buffer. Samples were centrifuged at 200,000 *g* for 2 h at 20 °C. The pellet was rinsed with 0.5% SB3–14 in PBS, resuspended in 50 μl of 0.5% SB3–14 in deionized water, and stored at −80 °C. Gel electrophoresis and silver staining were performed to assess the purity of brain extracts. To quantify PrP levels, samples were compared against a dilution series of recombinant PrP by immunoblotting and probing with the anti-PrP antibody POM19 (Polymenidou et al., 2008).

### 2.9. Heparan sulfate purification and analysis by mass spectrometry

Heparan sulfate (HS) was extracted from the purified PrP$^{Sc}$ preparation by anion exchange chromatography as described previously (Aguilar-Calvo et al., 2019). Purified PrP$^{Sc}$ was denatured in 0.5 M NaOH (final concentration) on ice at 4 °C for 16 h, neutralized with

0.5 M acetic acid (final concentration), and digested with pronase for 25 h at 37 °C. HS was then purified by diethyl-aminoethyl (DEAE) sepharose chromatography (Healthcare Life Sciences), and digested with 1 m-unit each of heparin lyases I, II, and III to depolymerize the HS chains. The disaccharides were then tagged by reductive amination with [$^{12}C_6$]aniline (Lawrence et al., 2008) and mixed with [$^{13}C_6$]aniline-tagged disaccharide standards. Samples were analyzed by liquid chromatography-mass spectrometry (LC-MS) using an LTQ Orbitrap Discovery electrospray ionization mass spectrometer (ThermoFisher Scientific). Internal disaccharides and nonreducing end monosaccharides were identified based on their unique mass and quantified relative to the HS weight (Lawrence et al., 2012; Lawrence et al., 2008).

### 2.10. Statistics

A Student's *t*-test (two-tailed, unpaired) was used to determine the statistical significance between the *Prnp*$^{187N}$*versus* WT mouse brain samples for the PrP$^{C}$ level of expression, levels of ADAM10-cleaved PrP$^{C}$ and PrP$^{Sc}$, as well as levels of HS bound to PrP$^{Sc}$ in ME7-infected WT and *Prnp*$^{187N}$ brains. One-way ANOVA with Tukey's post test was performed to assess survival differences between mouse groups. Two-way ANOVA with Bonferroni's post test was performed to assess differences in the lesion profiles, the glycoprofiles of PrP$^{Sc}$ in WT and *Prnp*$^{187N}$ mice infected with the four different PrP$^{Sc}$ strains, and the composition of HS bound to PrP$^{Sc}$ in ME7-infected *Prnp*$^{187N}$ and WT mouse brain. GraphPad Prism 5® software was used for statistical analyses. No measurement was excluded for statistical analysis. For all analyses, $P \leq .05$ was considered significant. Data displayed in graphs represent mean ± SEM.

### 2.11. Study approval

All animal studies were performed following procedures to minimize suffering and were approved by the Institutional Animal Care and Use Committee at UC San Diego. Protocols were performed in strict accordance with good animal practices, as described in the Guide for the Use and Care of Laboratory Animals published by the National Institutes of Health.

## 3. Results

### 3.1. Prnp$^{T187N}$ mice are highly susceptible to prion infection

To investigate how glycans impact prion conversion, we compared prion infection in WT and *Prnp*$^{187N}$ knockin mice, which express PrP with 0–2 or 0–3 N-linked glycans in the C-terminal globular domain of PrP, respectively. The *Prnp*$^{187N}$ mice have a third glycan at position 187 (mouse PrP numbering) from a single amino acid substitution (T187N) that creates a novel N-linked glycan sequon (NXS or NXT) (*T*VT to *N*VT) (Sevillano et al., 2020) (Fig. 1A). The glycan is located at the C-terminal end of helix 2, nearly equidistant between the two physiological glycans at positions 180 and 196 (Sevillano et al., 2020) (Fig. 1A, B).

We previously found that *Prnp*$^{187N}$ and WT mice express equivalent PrP$^{C}$ levels in the brain (Sevillano et al., 2020). The additional glycan altered PrP$^{187N}$ electrophoretic migration by approximately 2 kDa (Fig. 1C). Additionally, PrP$^{187N}$ was more highly glycosylated with significantly lower levels of the unglycosylated PrP glycoform (Fig. 1C). To measure PrP shed from the cell surface by ADAM10, we used a newly developed antibody (sPrP$^{G228}$) that specifically recognizes the new C-terminal epitope generated upon proteolytic cleavage (Linsenmeier et al., 2018). We found a 1.6-fold decrease in shed PrP, indicating reduced shedding of triglycosylated PrP$^{C}$ from the cell surface (Fig. 1C). Hence, in contrast to WT PrP$^{C}$, where the fully (di-) glycosylated form is the predominant substrate for ADAM10 (Fig. 1C) (Linsenmeier et al., 2018), an additional third glycan at position 187 impairs this cleavage, possibly due to steric hindrance.

To determine how a third glycan would impact prion conversion, neurodegeneration, and survival time, we inoculated mice intracerebrally with four distinct subfibrillar, mouse-adapted prion strains. On first passage, *Prnp*$^{187N}$ mice showed a 100% attack rate, but a markedly prolonged survival period compared to the WT mice (Fig. 2A, Table 1). However, by the second or third passage, three of four strains no longer showed a difference in survival time, indicating that the third glycan made little difference in conversion once the strain was adapted. For the RML-infected mice, the *Prnp*$^{187N}$ mice survived approximately 20% longer than WT mice (WT: 144 ± 5 days; *Prnp*$^{187N}$: 173 ± 5 days). The variance in the survival times among the *Prnp*$^{187N}$ mice infected with four prion strains was also similar to the WT mice (*Prnp*$^{187N}$: 155–207 days; WT: 140–205 days).

To assess how the third glycan affects the severity and regional distribution of neurodegeneration and gliosis, we scored eight brain regions for spongiform degeneration, gliosis, and PrP$^{Sc}$ deposition. Interestingly, RML-infected *Prnp*$^{187N}$ and WT brains displayed similar diffuse aggregate morphology (Fig. 2B) and the lesion profiles were nearly overlapping (Fig. 2C), despite a 30-day difference in the incubation period. The 22 L-infected *Prnp*$^{187N}$ brains also showed lesions that were nearly identical to WT (Fig. 2C). However, in *Prnp*$^{187N}$ mice infected with ME7 or mNS prions, there was a consistent decrease in the lesion severity, although the brain regions targeted were unchanged (Fig. 2B, C). The primary difference was a profound increase in the size of the plaque-like structures in the *Prnp*$^{187N}$ brains infected with ME7 prions [average plaque diameter 34 ± 2 μm (WT) *versus* 97 ± 6 μm *(Prnp*$^{187N}$*)*] and mNS prions [average plaque diameter 34 ± 2 μm (WT) *versus* 66 ± 6 μm *(Prnp*$^{187N}$*)*] (Fig. 2B).

ME7 and mNS prions typically form plaque-like structures and accumulate perineuronally in WT mice (Nilsson et al., 2010). We found that the cell tropism was similar in *Prnp*$^{187N}$ mice, as prions from either strain also accumulated perineuronally. Yet exclusively in the *Prnp*$^{187N}$ mice, neurons showed a prominent piling of prion aggregates extending outward from the surface, sometimes obscuring the neuron, suggesting a difference in the aggregate arrangement of highly glycosylated PrP (Fig. 2B). PrP$^{Sc}$ also frequently accumulated along the subarachnoid space and ventricular surfaces in the *Prnp*$^{187N}$ mice, potentially indicating PrP$^{Sc}$ transit through the interstitial fluid. Neuronal and meningeal aggregates were non-congophilic (Figs. 2D and S1) and periventricular aggregates were only rarely and focally congophilic (Fig. S1). To determine whether the PrP$^{Sc}$ was associated with extracellular vesicles (EVs), we co-immunolabelled brain sections for PrP and the tetraspanin and EV marker, CD9 (Fig. S2). Although PrP did not co-localize with CD9 in the WT mice, interestingly, there were focal PrP deposits that co-labelled with CD9 in the *Prnp*$^{187N}$ mice infected with ME7 or mNS prions, particularly periventricularly, suggesting that a subset of 187 N-PrP$^{Sc}$ may be attached to EVs (Fig. S2).

### 3.2. Triglycosylated PrP$^{Sc}$ is largely GPI-anchored and sediments slowly

We assessed the PrP$^{Sc}$ glycoform ratios by western blot and found that (1) all four strains converted tri-glycosylated PrP$^{C}$ into PK-resistant PrP$^{Sc}$ (Fig. 3A), and (2) unglycosylated PrP$^{Sc}$ levels were significantly lower for *Prnp*$^{187N}$ strains than for WT strains (Fig. 3A), potentially due to the lower levels of unglycosylated PrP$^{C}$ (Fig. 1C).

We previously found that mCWD plaques were enriched in ADAM10-cleaved PrP$^{Sc}$. To determine the levels of ADAM10-cleaved PrP$^{Sc}$ in ME7- and mNS-infected *Prnp*$^{187N}$ and WT brain, we immunoblotted PK-cleaved brain proteins using the sPrP$^{G228}$ antibody. We found that the cleaved PrP$^{Sc}$ levels were consistently lower by more than a log-fold as compared to mCWD, suggesting that PrP$^{Sc}$ in ME7- and mNS-infected brains remained largely GPI-anchored (Fig. 3B).

To next test whether the prions were internally cleaved as observed in genetic prion disease associated with the F198S-*PRNP* mutation, we probed PK-resistant PrP$^{Sc}$ with a series of antibodies against N- and C-terminal epitopes in PrP. However, no short internal fragments were

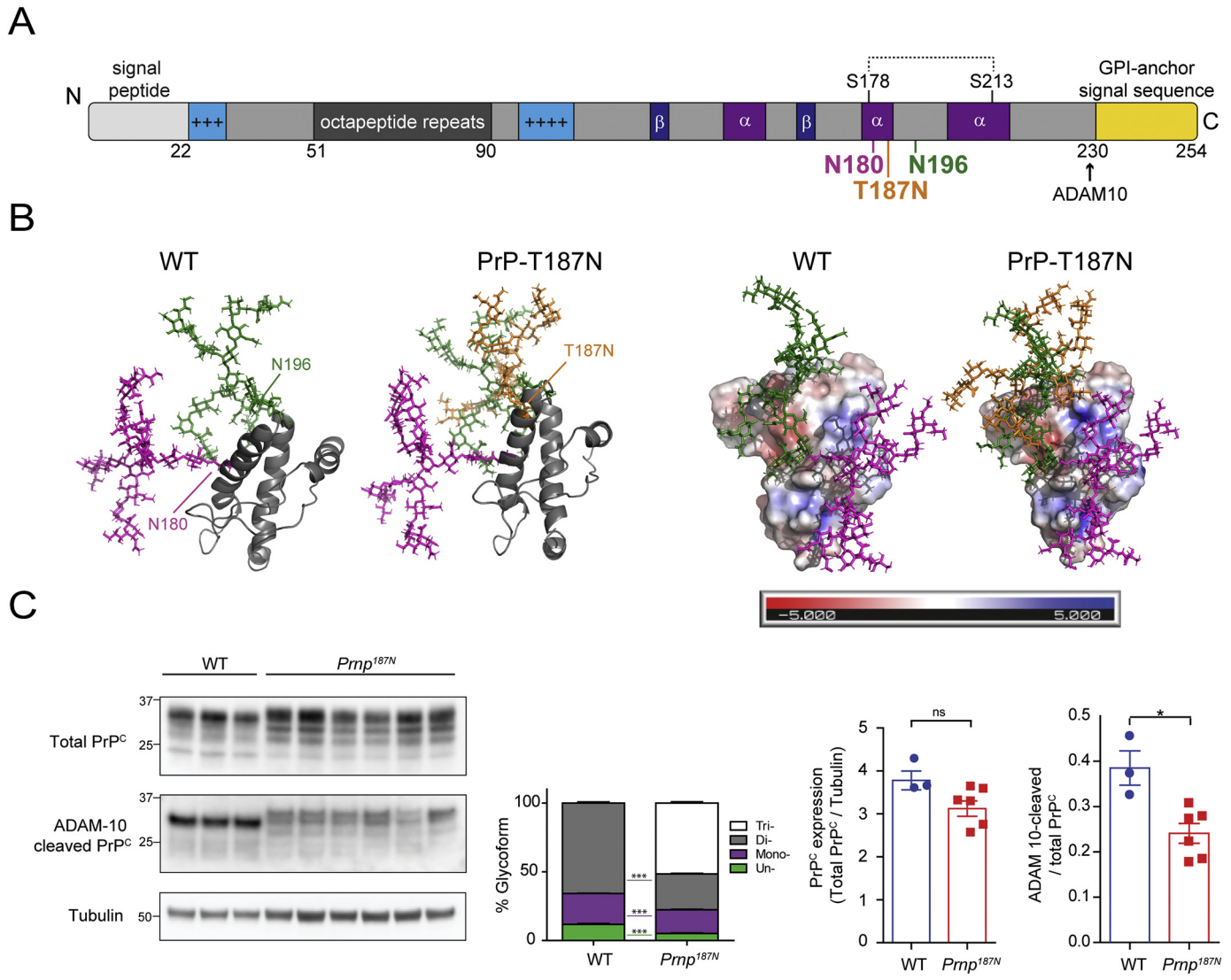


**Fig. 1. The T187N mutation introduces a third N-linked glycan to the globular C-terminal domain of PrP$^{C}$. A.** The PrP$^{C}$ primary structure shows the positively charged segments (light blue), $Cu^{2+}$-binding octapeptide repeats (dark grey), beta sheets (dark blue), alpha helices (purple), disulfide bond (dotted line), and GPI-anchor signal sequence (yellow). The glycans are linked to PrP residues 180N and 196N, and to the mutated 187N residue. **B.** Three-dimensional structure of the mature PrP$^{C}$ protein shown in ribbon form (left) or as a charged surface (right) (PDB ID code 1AG2). N-linked glycans attached to N180, N196, and N187 are depicted in magenta, green, and orange, respectively (note: tetra-antennary, terminally-sialylated glycans are shown (Katorcha and Baskakov, 2017; Rudd et al., 1999)). **C.** Western blots (left) show total and ADAM10-cleaved PrP$^{C}$ protein levels in whole brain lysates from adult WT or *Prnp$^{187N}$* mice. Graphs indicate relative percentages of each glycoform from total PrP: un- (green), mono- (purple), di- (grey), and tri-glycosylated (white) (mean ± SEM). Also quantified is ADAM10-cleaved PrP. $N$ = 3–6 mice per genotype. (For interpretation of the references to colour in this figure legend, the reader is referred to the web version of this article.)

evident for the ME7 strain, as the highly PK-resistant unglycosylated core fragment was consistently full length and the same molecular weight as WT PrP$^{Sc}$ (Fig. 3C), indicating that PrP was likely to be largely GPI-anchored and not a PrP fragment.

The glycans attached to PrP may impair fibril formation, restricting PrP$^{Sc}$ to small aggregates. To probe the sedimentation properties of highly glycosylated PrP$^{Sc}$, we performed velocity sedimentation on mNS- and ME7-infected brain samples, both of which displayed alterations in plaque morphology and lesion profiles in the *Prnp$^{187N}$* mice. We also performed velocity sedimentation on RML-infected brain, in order to include a strain that was not altered by the additional glycan. Brain homogenate was solubilized in a sarcosyl-based buffer, overlaid onto a 4–24% Optiprep™ step gradient, and centrifuged at 150,000 *g*. Interestingly, the tri-glycosylated mNS and ME7 prions sedimented in lighter fractions than the WT mNS and ME7 prions (Fig. 3D), suggesting that the tri-glycosylated mNS and ME7 prion aggregates were smaller or less compact than the less glycosylated WT prions. Additionally, the PrP$^{187N}$ aggregates were notably more homogenous and nearly monodispersed, as compared to the polydispersed particles in WT mice. By comparison, the RML prion particles from both mouse lines sedimented similarly (Fig. 3D).

### 3.3. Triglycosylated PrP$^{Sc}$ binds low levels of heparan sulfate

Glycosaminoglycans, including heparan sulfate (HS), co-localize with prion plaques in the brain (McBride et al., 1998; Snow et al., 1989b; Snow et al., 1990) and accelerate prion conversion *in vitro* (Wong et al., 2001). Unglycosylated PrP has a high heparin binding affinity and frequently forms HS-enriched congophilic plaques (Sevillano et al., 2020). Since the PrP$^{187N}$ aggregates formed non-congophilic, plaque-like deposits in the ME7- and mNS-infected mice, we next tested whether these prions bind HS. Using the antibody 10E4 that binds an N-sulfated glucosamine residue, we immunolabelled ME7 and mNS prion-infected brain sections for HS (Fig. 4A). Surprisingly, HS did

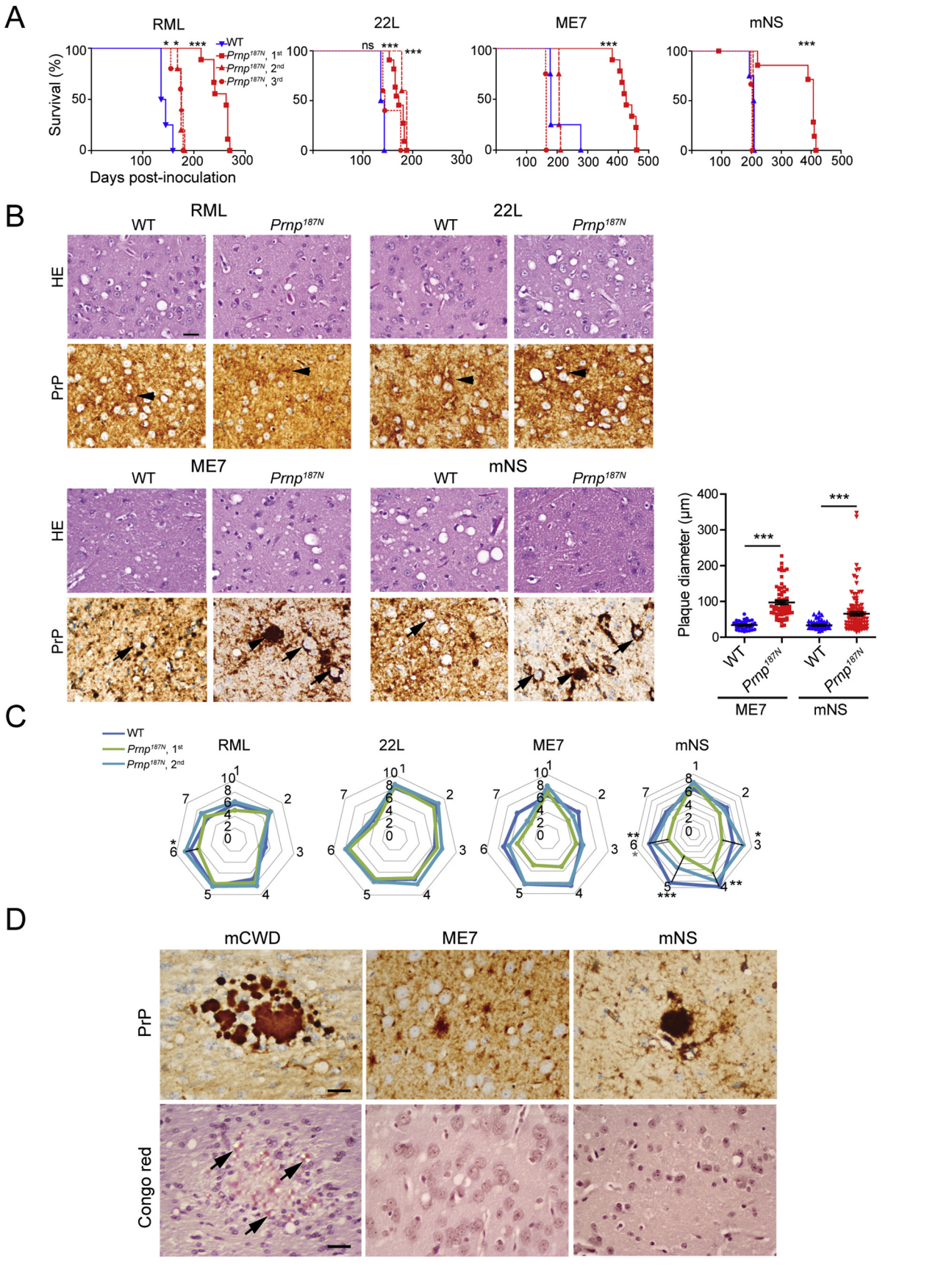


*(caption on next page)*

**Fig. 2. *Prnp*$^{187N}$mice initially show a prolonged survival time and plaque-like prion deposits in the brain for select strains. A.** Survival curves reveal a delayed time to the onset of terminal disease on the first passage for all strains, which decreased on subsequent passages. **B.** HE and PrP immunostains revealed similar spongiform degeneration and diffuse PrP$^{Sc}$ deposits in the RML and 22 L-infected WT and *Prnp*$^{187N}$ mice (arrowheads). Plaque-like deposits (arrowheads) were significantly larger in the ME7- and mNS-infected *Prnp*$^{187N}$ mice. Graph indicates plaque diameter (N = 3 mice per group, $n \geq 35$ plaques). Note the perineuronal prion deposits in the ME7 and mNS-infected WT and *Prnp*$^{187N}$ brain (arrows). **C.** Lesion profiles indicate the severity of spongiform change, astrogliosis, and PrP$^{Sc}$ deposition in 7 brain areas and are nearly superimposable for RML and 22 L-infected WT and *Prnp*$^{187N}$ mice. ME7- and mNS-infected mice showed less severe histopathologic lesions on first passage as compared to WT mice, however lesion severity increased by second passage (1-dorsal medulla, 2-cerebellum, 3-hypothalamus, 4-medial thalamus, 5-hippocampus, 6-cerebral cortex, 7-cerebral peduncles). For panel C: $n$ = 4–6 mice/group. **D.** Prion-like ME7 and mNS plaques in the *Prnp*$^{187N}$ brains are largely non-congophilic, unlike the mouse-adapted CWD prion strain (mCWD) used as a positive control. Brain regions shown in B: RML and 22 L, cerebral cortex; ME7 and mNS, thalamus, and (D) Congo red stain: mCWD, corpus callosum; ME7 and mNS, cerebral cortex. Scale bar = 50 μm (panel B). $^{*}P < .05$, $^{**}P < .01$, $^{***}P < .001$, Log-rank (Mantel-Cox) test (panel A), unpaired *t*-test (panel B), 2-way ANOVA with Bonferroni post (panel C). (For interpretation of the references to colour in this figure legend, the reader is referred to the web version of this article.)

**Table 1**
Incubation times for WT or *Prnp*$^{187N}$ mice inoculated with RML, 22 L, ME7, or mNS prion strains. Attack rate was 100% for all inoculated mice.

| Host | Prion | Passage | Number of mice | Incubation time Mean ± SEM (days) |
|---|---|---|---|---|
| WT | RML | | 4/4 | 144 ± 5 |
| *Prnp*$^{187N}$ | RML | 1 | 9/9 | 252 ± 6 |
| *Prnp*$^{187N}$ | *Prnp*$^{187N}$-RML | 2 | 5/5 | 175 ± 2 |
| *Prnp*$^{187N}$ | *Prnp*$^{187N}$-RML | 3 | 5/5 | 173 ± 5 |
| WT | 22 L | | 4/4 | 140 ± 2 |
| *Prnp*$^{187N}$ | 22 L | 1 | 11/11 | 173 ± 3 |
| *Prnp*$^{187N}$ | *Prnp*$^{187N}$-22 L | 2 | 5/5 | 184 ± 2 |
| *Prnp*$^{187N}$ | *Prnp*$^{187N}$-22 L | 3 | 5/5 | 155 ± 9 |
| WT | ME7 | | 4/4 | 203 ± 25 |
| *Prnp*$^{187N}$ | ME7 | 1 | 9/9 | 429 ± 9 |
| *Prnp*$^{187N}$ | *Prnp*$^{187N}$-ME7 | 2 | 4/4 | 207 ± 1 |
| *Prnp*$^{187N}$ | *Prnp*$^{187N}$-ME7 | 3 | 4/4 | 164 ± 1 |
| WT | mNS | | 4/4 | 205 ± 4 |
| *Prnp*$^{187N}$ | mNS | 1 | 7/7 | 428 ± 22 |
| *Prnp*$^{187N}$ | *Prnp*$^{187N}$-mNS | 2 | 5/5 | 205 ± 0 |
| *Prnp*$^{187N}$ | *Prnp*$^{187N}$-mNS | 3 | 3/3 | 200 ± 1 |

not co-localize with the PrP plaque-like deposits in the *Prnp*$^{187N}$-infected brain.

To confirm the lack of HS-PrP binding, we used liquid chromatography - mass spectrometry to quantify the HS levels and determine the HS composition bound to PrP$^{Sc}$ from the ME7-infected mice (Fig. 4B). We purified PrP$^{Sc}$ from WT and *Prnp*$^{187N}$ brains, measured PrP$^{Sc}$ levels compared to a dilution series of recombinant PrP by western blot (Fig. S3), assessed purity by silver stain, and then denatured and degraded the proteins by hydrolysis and enzyme digestion. HS was then purified and aniline tagged, and HS disaccharides were quantified by mass spectrometry compared to standards. We purified PrP$^{Sc}$ from *Prnp*$^{180Q,196Q}$ brains, which have previously been shown to bind high levels of HS, to include as a positive control (Sevillano et al., 2020). The amount of HS bound to PrP$^{Sc}$ from *Prnp*$^{187N}$ brains was not significantly different from WT, and both contained less HS than the PrP$^{Sc}$ purified from *Prnp*$^{180Q,196Q}$ brains. Additionally, the sulfation pattern of the HS bound to PrP$^{Sc}$ in all three samples was not significantly different.

Collectively, this data indicates that ME7 and mNS prions in *Prnp*$^{187N}$ mice form plaque-like deposits that are primarily GPI-anchored, Congo red negative, and HS-deficient, consistent with previous findings suggesting that HS does not bind highly glycosylated or GPI-anchored prions with high affinity, and with findings indicating that plaque-like structures observed in sporadic CJD maintain their GPI anchor (Zanusso et al., 2014).

## 4. Discussion

N-linked glycans stabilize proteins (Culyba et al., 2011; Feng et al., 2018; Price et al., 2012), including PrP, and slow prion fibril formation *in vitro*(Bosques and Imperiali, 2003). Here we tested whether the addition of a third glycan to PrP would slow prion disease progression *in vivo*, using *Prnp*$^{187N}$ knockin mice infected with four distinct prion strains. Our results instead demonstrate that *Prnp*$^{187N}$ mice remain highly susceptible to prions and show minimal changes in survival times, indicating that the additional glycan did not significantly hinder prion conversion.

The histopathology was markedly altered in the brains of *Prnp*$^{187N}$ mice infected with two of four prion strains, ME7 and mNS. PrP$^{Sc}$ typically accumulates as a thin band along neuronal cell membranes and as small plaque-like aggregates in WT mice. Instead, ME7 and mNS prions formed an extensive assembly of PrP$^{Sc}$ emerging from neuronal surfaces. These large plaque-like deposits differ from true amyloid plaques, as deposits were cell-associated, likely GPI-anchored, non-congophilic, and had low levels of bound HS. Notably, *Prnp*$^{180Q,196Q}$ mice expressing unglycosylated PrP develop a starkly different disease phenotype following ME7 and mNS infection, forming congophilic plaques composed of ADAM10-cleaved PrP highly enriched in HS (Sevillano et al., 2020). Collectively, these results indicate that certain prions can switch between true amyloid plaques and cell-associated plaque-like deposits, depending on the number of N-linked glycans on PrP$^{C}$ (zero or three). The subtle amino acid differences are unlikely to underlie the strain switch, as Tuzi and colleagues found that ME7 prion-infected *Prnp*$^{180T,196T}$ knockin mice, which also express unglycosylated PrP, similarly formed amyloid plaques (Tuzi et al., 2008).

### 4.1. Prion glycosylation inversely correlates with levels of PrP$^{Sc}$-bound heparan sulfate

Interestingly, early reports indicate that non-plaque deposits immunolabel minimally for HS, whereas amyloid plaques immunolabel strongly for HS in mice and in humans (Aguilar-Calvo et al., 2019; Sevillano et al., 2020; Snow et al., 1990). Indeed, previously we found that plaque formation and prion-bound HS levels measured by LC/MS were highly correlated (Aguilar-Calvo et al., 2019; Sevillano et al., 2020). Here, none of the four strains in the *Prnp*$^{187N}$ mice formed plaques enriched in HS, as had occurred in the *Prnp*$^{180Q,196Q}$ mice. Although *Prnp*$^{187N}$ mice formed plaque-like aggregates, the prion-bound HS levels were low, in agreement with previous findings suggesting that the N-linked glycans reduce the PrP binding affinity to sulfated glycosaminoglycans (Sevillano et al., 2020). Collectively, these results reinforce the concept that glycans diminish PrP interaction with HS cofactors, which may be limiting glycosylated prions to primarily oligomers.

### 4.2. PrP glycans promote aggregation on membranes to form large plaque-like structures

GPI-anchoring of PrP may hinder fibril formation, as mice expressing GPI-anchorless PrP consistently develop amyloid fibrils perivascularly following infection with diverse prion strains (Aguilar-Calvo et al., 2017; Chesebro et al., 2005). These findings, together with observations in human genetic prion disease associated with GPI-anchorless PrP (Ghetti et al., 1996a; Ghetti et al., 1996b; Ghetti et al., 1996c), have led to the suggestion that the GPI-anchor modulates fibril assembly of PrP, potentially through steric interference of fibril

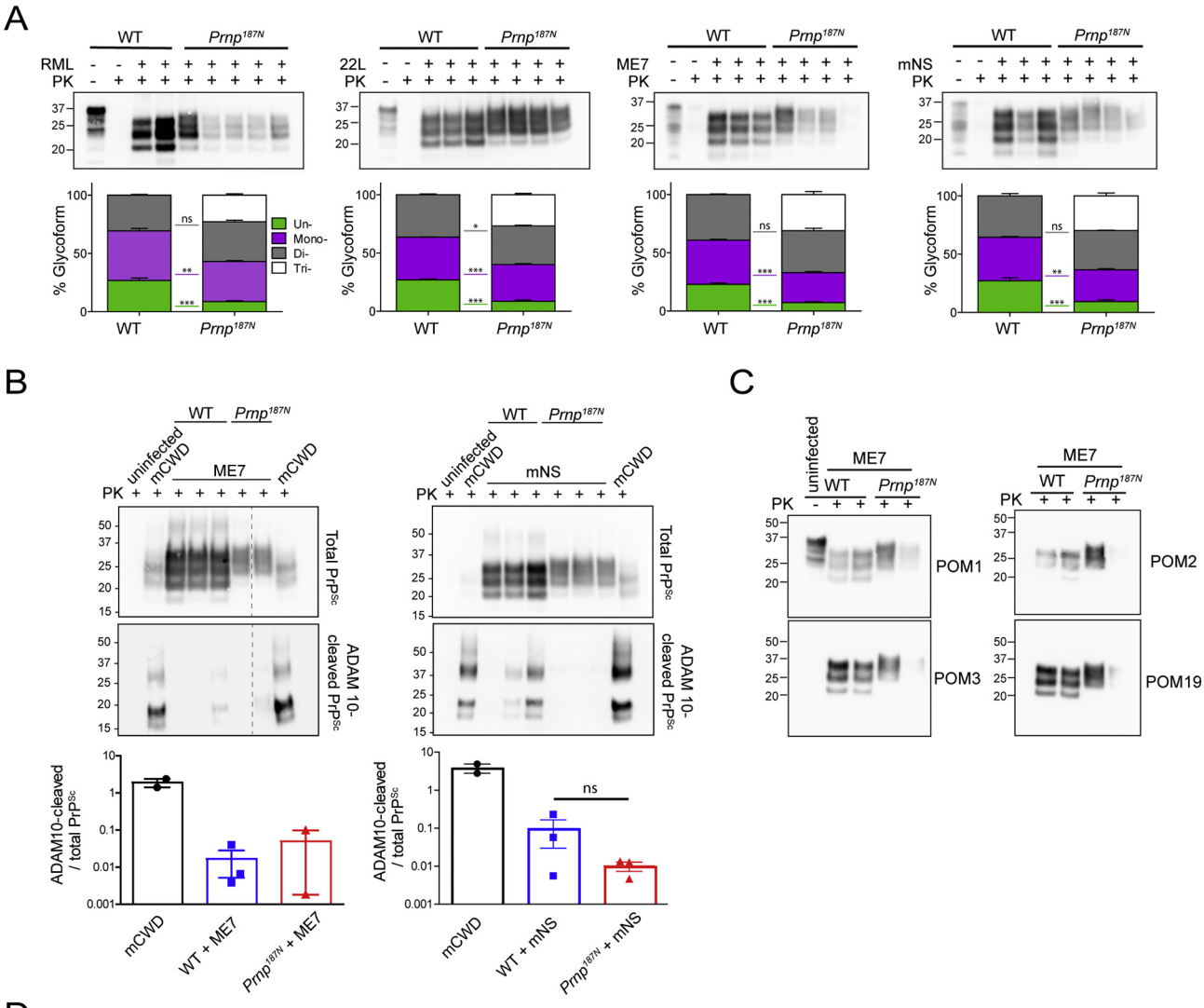


*(caption on next page)*

**Fig. 3. Biochemical properties of 187 N-PrP$^{Sc}$. A.** Electrophoretic mobility and glycoform profile of PrP$^{Sc}$ from RML-, 22 L-, ME7-, or mNS-prion-infected brain lysates (upper) show low levels of unglycosylated PrP$^{Sc}$ in the *Prnp$^{187N}$* mice brain. Lysates were treated with proteinase K (PK) where indicated to degrade PrP$^{C}$. Quantification of glycoforms (lower) show percentage of PrP$^{Sc}$ that contains zero (green), one (purple), two (grey), or three glycans (white). **B.** Representative western blots of ME7- or mNS-infected brain lysates from WT or *Prnp$^{187N}$* mice show total (upper) or ADAM10-cleaved PrP$^{Sc}$ shed from the cell surface (lower). Brain from mCWD-infected mice contain abundant ADAM10-cleaved PrP$^{Sc}$ (positive control) (Sevillano et al., 2020). Graphs show quantification (mean ± SE). **C.** Western blots show ME7-infected brain using antibodies against the octapeptide region of the PrP N-terminus (amino acids 53–88) (POM2), amino acids 95–100 (POM3), and a discontinuous epitope that includes the middle and distal C-terminus, which includes amino acid 220 (POM19) (Polymenidou et al., 2008). **D.** Western blots from a sedimentation velocity of RML, mNS, or ME7 prion-infected WT or *Prnp$^{187N}$* mice overlayed on a 4–24% Opti-prep™ step gradient, with the pellet fraction in the far right lane. Quantifications are shown below. N = 3–4 biological replicates per genotype for each strain, except for ME7-infected *Prnp$^{187N}$* shown in panel B ($N = 2$). (For interpretation of the references to colour in this figure legend, the reader is referred to the web version of this article.)

formation. To this end, a GPI-anchored form of the yeast prion, Sup35, expressed in neuronal cells formed membrane-bound, nonfibrillar aggregates, whereas GPI-anchorless Sup35 formed fibrils (Marshall et al., 2014). Interestingly, GPI-anchored Sup35 accumulated in extracellular vesicles piling on the cell surface, which may be relevant to our findings of extensive plaque-like deposits of ME7 and mNS prions piling on neuronal cell membranes. Considering that prions can be converted on the plasma membrane or in multivesicular bodies (MVB) (Caughey et al., 1991a; Yim et al., 2015), it is conceivable that ME7 and mNS prions accumulate in extracellular vesicles (EVs) (microvesicles or exosomes) that are trapped on the cell membrane. In this case, prions would retain the GPI-anchor, but would also be mobile and could transit through the interstitial and cerebrospinal fluid, accumulating periventricularly and adjacent to meninges, as we observed with PrP$^{Sc}$

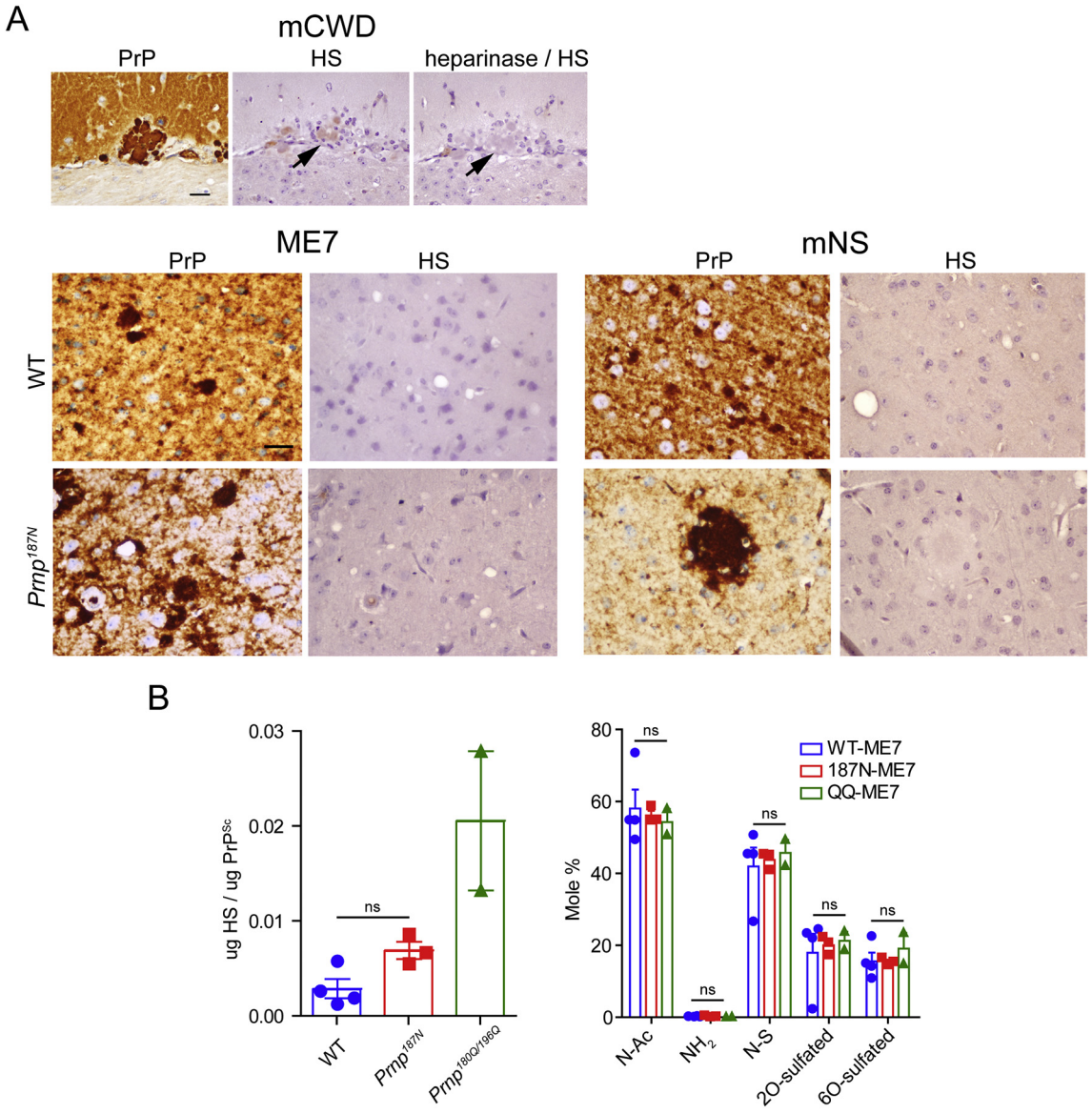


**Fig. 4. Heparan sulfate binding properties of PrP$^{187N}$. A.** ME7 and mNS plaque-like deposits in the WT and *Prnp$^{187N}$* brain sections do not label for HS using the anti-HS antibody 10E4, in contrast to amyloid plaques in the mCWD-infected brain (note that heparinase treatment ablates the HS labelling). **B.** Levels (left) and composition (right) of HS bound to PrP, as measured by LC-MS. Quantified are *N*-acetylated (N−Ac), unsubstituted glucosamine (NH2), N-sulfated (N-S), 2O-sulfated, and 6O-sulfated HS. Brain regions shown for HS stain in panel (A): ME7: cerebral cortex (WT) and thalamus (*Prnp$^{187N}$*); mNS: cerebral cortex (WT and *Prnp$^{187N}$*). Scale bar = 50 μm.

and CD9 co-localization. In support of this possibility, EVs have been shown to harbor prions and facilitate spread (Fevrier et al., 2004; Vella et al., 2007).

Previously $PrP^{Sc}$ was thought to retain the GPI-anchor, however, not all prions are exclusively GPI-anchored. For example, a plaque-forming prion, mCWD, is composed of monoglycosylated, shed PrP that lacks the GPI-anchor (Aguilar-Calvo et al., 2019). In humans with sporadic CJD, the presence of the GPI-anchor on plaque-like prion deposits has been controversial (Notari et al., 2008; Zanusso et al., 2014), with recent biochemical studies indicating thatprion deposits are composed of GPI-anchored PrP (Zanusso et al., 2014). Taken together, our data suggest that the two PrP N-linked glycans favor the conversion of GPI-anchored small or compact oligomers that bind poorly to HS, accumulating as diffuse and plaque-like deposits associated with cells and at sites of interstitial and CSF efflux. Future studies to determine whether the plaque-like deposits originate from surface-associated microvesicles budding from the cell surface, from released MVB-derived exosomes, or from another source will provide insight into subcellular prion conversion sites and the rapid dissemination of human and animal prions.

Supplementary data to this article can be found online at https://doi.org/10.1016/j.nbd.2020.104955.

## Authors' contributions

JAC, AMS, TDK, and CJS conceived the study and designed the experiments, HA and MG provided reagents, JAC, AMS, KS, TDK, TS, and DPP performed the experiments, JAC, AMS, and JDE conducted the data analysis, and JAC and CJS wrote the manuscript, with input from AMS, HA, MG, and JDE.

## Declaration of Competing Interests

The authors declare no competing financial interests.

## Acknowledgements

We thank Jin Wang and Taylor Winrow for outstanding technical support, and the animal care staff at UC San Diego for excellent animal care. We thank the UC San Diego GlycoAnalytics Core for the mass spectrometry analysis, and Dr. Patricia Aguilar-Calvo for critical review of the manuscript. This study was supported by the National Institutes of Health grants NS069566 (CJS), NS076896 (CJS), K12HL141956 (JAC), CJD Foundation (CJS and HA), and the Werner-Otto-Stiftung (HA).

## References

Aguilar-Calvo, P., Xiao, X., Bett, C., Erana, H., Soldau, K., Castilla, J., Nilsson, K.P., Surewicz, W.K., Sigurdson, C.J., 2017. Post-translational modifications in PrP expand the conformational diversity of prions in vivo. Sci. Rep. 7, 43295. https://doi.org/10.1038/srep43295.

Aguilar-Calvo, P., Sevillano, A.M., Bapat, J., Soldau, K., Sandoval, D.R., Altmeppen, H.C., Linsenmeier, L., Pizzo, D.P., Geschwind, M.D., Sanchez, H., et al., 2019. Shortening heparan sulfate chains prolongs survival and reduces parenchymal plaques in prion disease caused by mobile, ADAM10-cleaved prions. Acta Neuropathol: Doi. https://doi.org/10.1007/s00401-019-02085-x.

Aguzzi, A., Lakkaraju, A.K., 2016. Cell biology of prions and Prionoids: a status report. Trends Cell Biol. 26, 40–51. https://doi.org/10.1016/j.tcb.2015.08.007.

Baiardi, S., Rossi, M., Capellari, S., Parchi, P., 2019. Recent advances in the histo-molecular pathology of human prion disease. Brain Pathol. 29, 278–300. https://doi.org/10.1111/bpa.12695.

Baldwin, M.A., Stahl, N., Reinders, L.G., Gibson, B.W., Prusiner, S.B., Burlingame, A.L., 1990. Permethylation and tandem mass spectrometry of oligosaccharides having free hexosamine: analysis of the glycoinositol phospholipid anchor glycan from the scrapie prion protein. Anal. Biochem. 191, 174–182.

Baron, G.S., Hughson, A.G., Raymond, G.J., Offerdahl, D.K., Barton, K.A., Raymond, L.D., Dorward, D.W., Caughey, B., 2011. Effect of glycans and the glycophosphatidylinositol anchor on strain dependent conformations of scrapie prion protein: improved purifications and infrared spectra. Biochemistry 50, 4479–4490. https://doi.org/10.1021/bi2003907.

Bosques, C.J., Imperiali, B., 2003. The interplay of glycosylation and disulfide formation influences fibrillization in a prion protein fragment. Proc. Natl. Acad. Sci. U. S. A. 100, 7593–7598. https://doi.org/10.1073/pnas.1232504100.

Bruce, M.E., 1993. Scrapie strain variation and mutation. Br. Med. Bull. 49, 822–838.

Bruce, M.E., Dickinson, A.G., 1979. Biological stability of different classes of scrapie agent. In slow virus infections of the central nervous system. In: Prusiner, S.B., Hadlow, W.H. (Eds.), Slow Virus Infections of the Central Nervous System. Academic Press, City, New York, pp. 71–86.

Burke, C.M., Walsh, D.J., Steele, A.D., Agrimi, U., Di Bari, M.A., Watts, J.C., Supattapone, S., 2019. Full restoration of specific infectivity and strain properties from pure mammalian prion protein. PLoS Pathog. 15, e1007662. https://doi.org/10.1371/journal.ppat.1007662.

Caughey, B., Raymond, G.J., Ernst, D., Race, R.E., 1991a. N-terminal truncation of the scrapie-associated form of PrP by lysosomal protease(s): implications regarding the site of conversion of PrP to the protease-resistant state. J. Virol. 65, 6597–6603.

Caughey, B.W., Dong, A., Bhat, K.S., Ernst, D., Hayes, S.F., Caughey, W.S., 1991b. Secondary structure analysis of the scrapie-associated protein PrP 27-30 in water by infrared spectroscopy [published erratum appears in biochemistry 1991 Oct 29;30(43):10600]. Biochemistry 30, 7672–7680.

Chesebro, B., Race, R., Wehrly, K., Nishio, J., Bloom, M., Lechner, D., Bergstrom, S., Robbins, K., Mayer, L., Keith, J.M., 1985. Identification of scrapie prion protein-specific mRNA in scrapie-infected and uninfected brain. Nature 315, 331–333.

Chesebro, B., Trifilo, M., Race, R., Meade-White, K., Teng, C., LaCasse, R., Raymond, L., Favara, C., Baron, G., Priola, S., et al., 2005. Anchorless prion protein results in infectious amyloid disease without clinical scrapie. Science 308, 1435–1439.

Culyba, E.K., Price, J.L., Hanson, S.R., Dhar, A., Wong, C.H., Gruebele, M., Powers, E.T., Kelly, J.W., 2011. Protein native-state stabilization by placing aromatic side chains in N-glycosylated reverse turns. Science 331, 571–575. https://doi.org/10.1126/science.1198461.

Deleault, N.R., Harris, B.T., Rees, J.R., Supattapone, S., 2007. Formation of native prions from minimal components in vitro. Proc. Natl. Acad. Sci. U. S. A. 104, 9741–9746.

Dickinson, A.G., 1976. Scrapie in sheep and goats. Front. Biol. 44, 209–241.

Dickinson, A.W., Outram, G.W., Taylor, D.M., Foster, J.D., 1986. Further evidence that scrapie agent has an independent genome. In: In Court, L.A., Dormont, D., Brown, P., Kingsbury, D.T. (Eds.), Unconventional Virus Diseases of the Central Nervous System. Commisariat à l'Energie Atomique, Paris, France, City, pp. 446–460.

Endo, T., Groth, D., Prusiner, S.B., Kobata, A., 1989. Diversity of oligosaccharide structures linked to asparagines of the scrapie prion protein. Biochemistry 28, 8380–8388.

Feng, X., Wang, X., Han, B., Zou, C., Hou, Y., Zhao, L., Li, C., 2018. Design of Glyco-Linkers at multiple structural levels to modulate protein stability. J. Phys. Chem. Lett. 9, 4638–4645. https://doi.org/10.1021/acs.jpclett.8b01570.

Fevrier, B., Vilette, D., Archer, F., Loew, D., Faigle, W., Vidal, M., Laude, H., Raposo, G., 2004. Cells release prions in association with exosomes. Proc. Natl. Acad. Sci. U. S. A. 101, 9683–9688.

Ghetti, B., Piccardo, P., Frangione, B., Bugiani, O., Giaccone, G., Young, K., Prelli, F., Farlow, M.R., Dlouhy, S.R., Tagliavini, F., 1996a. Prion Protein Amyloidosis. Brain Pathol. 6, 127–145.

Ghetti, B., Piccardo, P., Frangione, B., Bugiani, O., Giaccone, G., Young, K., Prelli, F., Farlow, M.R., Dlouhy, S.R., Tagliavini, F., 1996b. Prion protein hereditary amyloidosis - parenchymal and vascular. Semin. Virol. 7, 189–200.

Ghetti, B., Piccardo, P., Spillantini, M.G., Ichimiya, Y., Porro, M., Perini, F., Kitamoto, T., Tateishi, J., Seiler, C., Frangione, B., et al., 1996c. Vascular variant of prion protein cerebral amyloidosis with tau-positive neurofibrillary tangles: the phenotype of the stop codon 145 mutation in PRNP. Proc. Natl. Acad. Sci. U. S. A. 93, 744–748.

Ghetti, B., Piccardo, P., Zanusso, G., 2018. Dominantly inherited prion protein cerebral amyloidoses - a modern view of Gerstmann-Straussler-Scheinker. Handb. Clin. Neurol. 153, 243–269. https://doi.org/10.1016/b978-0-444-63945-5.00014-3.

Greenlee, J.J., Greenlee, M.H., 2015. The transmissible spongiform encephalopathies of livestock. ILAR J. 56, 7–25. https://doi.org/10.1093/ilar/ilv008.

Group. W, 2020. GLYCAM Web. Complex Carbohydrate Research Center. http://glycam.org.

Iwasaki, Y., Kato, H., Ando, T., Mimuro, M., Kitamoto, T., Yoshida, M., 2017. MM1-type sporadic Creutzfeldt-Jakob disease with 1-month total disease duration and early pathologic indicators. Neuropathology 37, 420–425. https://doi.org/10.1111/neup.12379.

Jucker, M., Walker, L.C., 2018. Propagation and spread of pathogenic protein assemblies in neurodegenerative diseases. Nat. Neurosci. 21, 1341–1349. https://doi.org/10.1038/s41593-018-0238-6.

Katorcha, E., Baskakov, I.V., 2017. Analyses of N-linked glycans of PrP(Sc) revealed predominantly 2,6-linked sialic acid residues. FEBS J. 284, 3727–3738. https://doi.org/10.1111/febs.14268.

Kim, M.O., Takada, L.T., Wong, K., Forner, S.A., Geschwind, M.D., 2018. Genetic PrP prion diseases. Cold Spring Harb. Perspect. Biol. 10. https://doi.org/10.1101/cshperspect.a033134.

Kovacs, G.G., 2019. Molecular pathology of neurodegenerative diseases: principles and practice. J. Clin. Pathol. 72, 725–735. https://doi.org/10.1136/jclinpath-2019-205952.

Lawrence, R., Olson, S.K., Steele, R.E., Wang, L., Warrior, R., Cummings, R.D., Esko, J.D., 2008. Evolutionary differences in glycosaminoglycan fine structure detected by quantitative glycan reductive isotope labeling. J. Biol. Chem. 283, 33674–33684. https://doi.org/10.1074/jbc.M804288200.

Lawrence, R., Brown, J.R., Al-Mafraji, K., Lamanna, W.C., Beitel, J.R., Boons, G.J., Esko, J.D., Crawford, B.E., 2012. Disease-specific non-reducing end carbohydrate biomarkers for mucopolysaccharidoses. Nat. Chem. Biol. 8, 197–204. Doi nchembio.766 [pii]. https://doi.org/10.1038/nchembio.766.

Linsenmeier, L., Mohammadi, B., Wetzel, S., Puig, B., Jackson, W.S., Hartmann, A., Uchiyama, K., Sakaguchi, S., Endres, K., Tatzelt, J., et al., 2018. Structural and

mechanistic aspects influencing the ADAM10-mediated shedding of the prion protein. Mol. Neurodegener. 13, 18. https://doi.org/10.1186/s13024-018-0248-6.
Marshall, K.E., Offerdahl, D.K., Speare, J.O., Dorward, D.W., Hasenkrug, A., Carmody, A.B., Baron, G.S., 2014. Glycosylphosphatidylinositol anchoring directs the assembly of Sup35NM protein into non-fibrillar, membrane-bound aggregates. J. Biol. Chem. 289, 12245–12263. https://doi.org/10.1074/jbc.M114.556639.
McBride, P.A., Wilson, M.I., Eikelenboom, P., Tunstall, A., Bruce, M.E., 1998. Heparan sulfate proteoglycan is associated with amyloid plaques and neuroanatomically targeted PrP pathology throughout the incubation period of scrapie-infected mice. Exp. Neurol. 149, 447–454.
Mitra, N., Sinha, S., Ramya, T.N., Surolia, A., 2006. N-linked oligosaccharides as outfitters for glycoprotein folding, form and function. Trends Biochem. Sci. 31, 156–163. https://doi.org/10.1016/j.tibs.2006.01.003.
Nilsson, K.P., Joshi-Barr, S., Winson, O., Sigurdson, C.J., 2010. Prion strain interactions are highly selective. J. Neurosci. 30, 12094–12102. Doi 30/36/12094 [pii]. https://doi.org/10.1523/JNEUROSCI.2417-10.2010.
Notari, S., Strammiello, R., Capellari, S., Giese, A., Cescatti, M., Grassi, J., Ghetti, B., Langeveld, J.P., Zou, W.Q., Gambetti, P., et al., 2008. Characterization of truncated forms of abnormal prion protein in Creutzfeldt-Jakob disease. J. Biol. Chem. 283, 30557–30565. https://doi.org/10.1074/jbc.M801877200.
Oesch, B., Westaway, D., Walchli, M., McKinley, M.P., Kent, S.B., Aebersold, R., Barry, R.A., Tempst, P., Teplow, D.B., Hood, L.E., et al., 1985. A cellular gene encodes scrapie PrP 27-30 protein. Cell 40, 735–746.
Peretz, D., Scott, M.R., Groth, D., Williamson, R.A., Burton, D.R., Cohen, F.E., Prusiner, S.B., 2001. Strain-specified relative conformational stability of the scrapie prion protein. Protein Sci. 10, 854–863.
Polymenidou, M., Moos, R., Scott, M., Sigurdson, C., Shi, Y.Z., Yajima, B., Hafner-Bratkovic, I., Jerala, R., Hornemann, S., Wuthrich, K., et al., 2008. The POM monoclonals: a comprehensive set of antibodies to non-overlapping prion protein epitopes. PLoS One 3, e3872. https://doi.org/10.1371/journal.pone.0003872.
Price, J.L., Powers, D.L., Powers, E.T., Kelly, J.W., 2011. Glycosylation of the enhanced aromatic sequon is similarly stabilizing in three distinct reverse turn contexts. Proc. Natl. Acad. Sci. U. S. A. 108, 14127–14132. https://doi.org/10.1073/pnas.1105880108.
Price, J.L., Culyba, E.K., Chen, W., Murray, A.N., Hanson, S.R., Wong, C.H., Powers, E.T., Kelly, J.W., 2012. N-glycosylation of enhanced aromatic sequons to increase glycoprotein stability. Biopolymers 98, 195–211. https://doi.org/10.1002/bip.22030.
Prusiner, S.B., 1982. Novel proteinaceous infectious particles cause scrapie. Science 216, 136–144.
Prusiner, S.B., Scott, M., Foster, D., Pan, K.M., Groth, D., Mirenda, C., Torchia, M., Yang, S.L., Serban, D., Carlson, G.A., et al., 1990. Transgenetic studies implicate interactions between homologous PrP isoforms in scrapie prion replication. Cell 63, 673–686.
Raymond, G.J., Chabry, J., 2004. Methods and tools in biosciences and medicine. In: Lehmann, S., Grassi, J. (Eds.), Techniques in Prion Research. Birkhäuser, Basel, City, pp. 16–26.
Riek, R., Hornemann, S., Wider, G., Billeter, M., Glockshuber, R., Wuthrich, K., 1996. Nmr structure of the mouse prion protein domain Prp(121 − 231). Nature 382, 180–182.
Rudd, P.M., Endo, T., Colominas, C., Groth, D., Wheeler, S.F., Harvey, D.J., Wormald, M.R., Serban, H., Prusiner, S.B., Kobata, A., et al., 1999. Glycosylation differences between the normal and pathogenic prion protein isoforms. Proc. Natl. Acad. Sci. U. S. A. 96, 13044–13049.
Rudd, P.M., Wormald, M.R., Wing, D.R., Prusiner, S.B., Dwek, R.A., 2001. Prion glycoprotein: structure, dynamics, and roles for the sugars. Biochemistry 40, 3759–3766.
Sandberg, M.K., Al-Doujaily, H., Sharps, B., Clarke, A.R., Collinge, J., 2011. Prion propagation and toxicity in vivo occur in two distinct mechanistic phases. Nature 470, 540–542. https://doi.org/10.1038/nature09768.
Selkoe, D.J., 1991. The molecular pathology of Alzheimer's disease. Neuron 6, 487–498.
Sevillano, A.M., Aguilar-Calvo, P., Kurt, T.D., Lawrence, J.A., Soldau, K., Nam, T.H., Schumann, T., Pizzo, D.P., Nystrom, S., Choudhury, B., et al., 2020. Prion protein glycans reduce intracerebral fibril formation and spongiosis in prion disease. J. Clin. Invest. https://doi.org/10.1172/jci131564.
Sigurdson, C.J., Manco, G., Schwarz, P., Liberski, P., Hoover, E.A., Hornemann, S., Polymenidou, M., Miller, M.W., Glatzel, M., Aguzzi, A., 2006. Strain fidelity of chronic wasting disease upon murine adaptation. J. Virol. 80, 12303–12311. https://doi.org/10.1128/jvi.01120-06.
Sim, V.L., Caughey, B., 2008. Ultrastructures and Strain Comparison of under-Glycosylated Scrapie Prion Fibrils. Neurobiol. Aging. https://doi.org/10.1016/j.neurobiolaging.2008.02.016. Doi S0197-4580(08)00065-1 [pii].
Snow, A.D., Kisilevsky, R., Willmer, J., Prusiner, S.B., DeArmond, S.J., 1989a. Sulfated glycosaminoglycans in amyloid plaques of prion diseases. Acta Neuropathol. 77, 337–342.
Snow, A.D., Kisilevsky, R., Willmer, J., Prusiner, S.B., DeArmond, S.J., 1989b. Sulfated glycosaminoglycans in amyloid plaques of prion diseases. Acta Neuropathol Berl 77, 337–342.
Snow, A.D., Wight, T.N., Nochlin, D., Koike, Y., Kimata, K., DeArmond, S.J., Prusiner, S.B., 1990. Immunolocalization of heparan sulfate proteoglycans to the prion protein amyloid plaques of Gerstmann-Straussler syndrome, Creutzfeldt-Jakob disease and scrapie. Lab. Investig. 63, 601–611.
Srivastava, S., Katorcha, E., Daus, M.L., Lasch, P., Beekes, M., Baskakov, I.V., 2017. Sialylation controls prion fate in vivo. J. Biol. Chem. 292, 2359–2368. https://doi.org/10.1074/jbc.M116.768010.
Srivastava, S., Katorcha, E., Makarava, N., Barrett, J.P., Loane, D.J., Baskakov, I.V., 2018. Inflammatory response of microglia to prions is controlled by sialylation of PrP(Sc). Sci. Rep. 8, 11326. https://doi.org/10.1038/s41598-018-29720-z.
Stahl, N., Baldwin, M.A., Prusiner, S.B., 1991. Electrospray mass spectrometry of the glycosylinositol phospholipid of the scrapie prion protein. Cell Biol Int Rep 15, 853–862.
Stohr, J., Weinmann, N., Wille, H., Kaimann, T., Nagel-Steger, L., Birkmann, E., Panza, G., Prusiner, S.B., Eigen, M., Riesner, D., 2008. Mechanisms of prion protein assembly into amyloid. Proc. Natl. Acad. Sci. U. S. A. 105, 2409–2414. https://doi.org/10.1073/pnas.0712036105.
Tuzi, N.L., Cancellotti, E., Baybutt, H., Blackford, L., Bradford, B., Plinston, C., Coghill, A., Hart, P., Piccardo, P., Barron, R.M., et al., 2008. Host PrP glycosylation: a major factor determining the outcome of prion infection. PLoS Biol. 6, e100. Doi 07-PLBI-RA-2655 [pii]. https://doi.org/10.1371/journal.pbio.0060100.
Vaquer-Alicea, J., Diamond, M.I., 2019. Propagation of protein aggregation in neurodegenerative diseases. Annu. Rev. Biochem. 88, 785–810. https://doi.org/10.1146/annurev-biochem-061516-045049.
Varki, A., 2017. Biological roles of glycans. Glycobiology 27, 3–49. https://doi.org/10.1093/glycob/cww086.
Vella, L.J., Sharples, R.A., Lawson, V.A., Masters, C.L., Cappai, R., Hill, A.F., 2007. Packaging of prions into exosomes is associated with a novel pathway of PrP processing. J. Pathol. 211, 582–590. https://doi.org/10.1002/path.2145.
Wadsworth, J.D.F., Joiner, S., Hill, A.F., Campbell, T.A., Desbruslais, M., Luthert, P.J., Collinge, J., 2001. Tissue distribution of protease resistant prion protein in variant CJD using a highly sensitive immuno-blotting assay. Lancet 358, 171–180.
Wang, F., Wang, X., Yuan, C.G., Ma, J., 2010. Generating a prion with bacterially expressed recombinant prion protein. Science 327, 1132–1135. Doi science.1183748 [pii]. https://doi.org/10.1126/science.1183748.
Weerapana, E., Imperiali, B., 2006. Asparagine-linked protein glycosylation: from eukaryotic to prokaryotic systems. Glycobiology 16, 91r–101r. https://doi.org/10.1093/glycob/cwj099.
Wong, C., Xiong, L.W., Horiuchi, M., Raymond, L., Wehrly, K., Chesebro, B., Caughey, B., 2001. Sulfated glycans and elevated temperature stimulate PrP(Sc)-dependent cell-free formation of protease-resistant prion protein. EMBO J. 20, 377–386.
Yim, Y.I., Park, B.C., Yadavalli, R., Zhao, X., Eisenberg, E., Greene, L.E., 2015. The multivesicular body is the major internal site of prion conversion. J. Cell Sci. 128, 1434–1443. https://doi.org/10.1242/jcs.165472.
Zanusso, G., Fiorini, M., Ferrari, S., Meade-White, K., Barbieri, I., Brocchi, E., Ghetti, B., Monaco, S., 2014. Gerstmann-Straussler-Scheinker disease and "anchorless prion protein" mice share prion conformational properties diverging from sporadic Creutzfeldt-Jakob disease. J. Biol. Chem. 289, 4870–4881. https://doi.org/10.1074/jbc.M113.531335.
Zerr, I., Parchi, P., 2018. Sporadic Creutzfeldt-Jakob disease. Handb. Clin. Neurol. 153, 155–174. https://doi.org/10.1016/b978-0-444-63945-5.00009-x.
Zerr, I., Schulz-Schaeffer, W.J., Giese, A., Bodemer, M., Schroter, A., Henkel, K., Tschampa, H.J., Windl, O., Pfahlberg, A., Steinhoff, B.J., et al., 2000. Current clinical diagnosis in Creutzfeldt-Jakob disease: identification of uncommon variants. Ann. Neurol. 48, 323–329.